Compensation of Strong Thermal Lensing in High-Optical-Power Cavities

C. Zhao, J. Degallaix, L. Ju, Y. Fan, and D. G. Blair
School of Physics, The University of Western Australia, 35 Stirling Highway, Nedlands, Western Australia 6009, Australia

B. J. J. Slagmolen, M. B. Gray, C. M. Mow Lowry, and D. E. McClelland
Centre for Gravitational Physics, The Australian National University, Canberra, 0200, Australia

D. J. Hosken, D. Mudge, A. Brooks, J. Munch, and P. J. Veitch
Department of Physics, The University of Adelaide, Adelaide, South Australia, 5005 Australia

M. A. Barton and G. Billingsley
LIGO, California Institute of Technology, Pasadena, California 91125, USA
(Received 28 February 2006)

In an experiment to simulate the conditions in high optical power advanced gravitational wave detectors, we show for the first time that the time evolution of strong thermal lenses follows the predicted infinite sum of exponentials (approximated by a double exponential), and that such lenses can be compensated using an intracavity compensation plate heated on its cylindrical surface. We show that high finesse ~1400 can be achieved in cavities with internal compensation plates, and that mode matching can be maintained. The experiment achieves a wave front distortion similar to that expected for the input test mass substrate in the Advanced Laser Interferometer Gravitational Wave Observatory, and shows that thermal compensation schemes are viable. It is also shown that the measurements allow a direct measurement of substrate optical absorption in the test mass and the compensation plate.

DOI: PACS numbers: 04.80.Nn, 95.55.Ym

The first generation laser interferometer gravitational wave detectors are taking data [1–5]. The Laser Interferometer Gravitational Wave Observatory (LIGO) detectors have achieved their target design sensitivity, and yet this sensitivity is estimated to be only sufficient to detect large rare gravitational wave signals. To achieve frequent detection of signals from firmly predicted sources, a tenfold improvement in sensitivity is required. This will increase the sensitive range from ~14 Mpc today to about 200 Mpc, leading to event rates of many per year [6].

To achieve this improvement the Advanced LIGO [7] and other second generation detectors require a ~100-fold increase in circulating laser power, in addition to improvement in the interferometer configuration, test mass thermal noise, and vibration isolation. This high power level is proposed to be achieved as follows: 125 W of stabilized laser power is injected into the interferometer. This is built up to ~2 KW inside the power recycling cavity and a further enhanced to more than 800 kW in the 4 km long Fabry-Perot arm cavities. Such power levels create two significant challenges. The first is to control parametric instabilities in the form of radiation pressure mediated opto-mechanical oscillation [8]. The second is the control of strong thermal lensing in the beam splitter (BS) and inboard test mass (ITM), which is the topic of this Letter. Figure 1 [7] shows the core optical components of an advanced interferometer, with shading showing the temperature build up in the core optical components. Thermal lensing arises whenever absorbed light in an optical substrate or coating creates a temperature gradient, which, via thermal expansion and the thermo-optic coefficient, leads to wave front distortion of the optical modes of the interferometer [9–15].

In the Advanced LIGO the absorption in the ITM substrate and coatings is predicted to create a strong thermal lens with focal length ~4.9 km [16], which is comparable to the ITM mirror focal length of 1.038 km. Such strong thermal lensing will normally cause an interferometer to either severely lose sensitivity or become inoperable [10]. Already, compensation of thermal lensing due to excess absorption in an ITM has been required in the initial LIGO

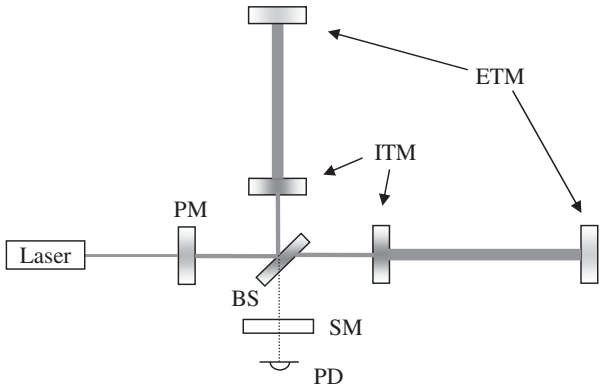

FIG. 1. Simplified schematic diagram of the optical layout of an advanced interferometer: ETM, ITM, power recycling mirror (PM), signal recycling mirror (SM), BS, photodiode (PD). Shading illustrates the thermal lensing in the various components; the beamwidth signifies light intensity.

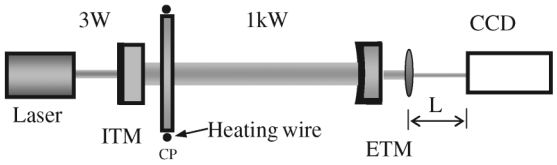

FIG. 2. A schematic diagram of the experiment setup. The beam from 10 W laser is mode matched into the Fabry-Perot cavity formed by the back-surface ITM and the ETM. The CP is placed near the ITM and heated by 6 turns of nichrome wire insulated by Teflon tape. The Fourier transform of the beam transmitted through the ETM is recorded by a CCD camera placed near the back focal plane of the 50 mm diameter, 500 mm focal length lens.

interferometer [17,18]. In that case, a CO_2 laser beam was used to heat the back surface of the ITM to cancel the positive lens produced by absorption. Similar low level compensation has been applied to the GEO 600 gravitational wave detector [19].

In this Letter we report on the observation and characterization of strong thermal lensing in a sapphire ITM, in which the magnitude of the distortion is similar to that expected in the Advanced LIGO. We demonstrate compensation using direct heating of a fused silica compensation plate inside the cavity. We show for the first time that the thermal lens evolves according to the predictions of Hello and Vinet [13], and show that the results may be used to determine the average optical absorption of both the test mass and the compensation plate.

The experiment described here was performed at the Gingin High Optical Power Test Facility (HOPTF) [20] in Western Australia, which has been developed with the specific goal of investigating the effects of high optical power as part of the LIGO collaboration [21]. It has a maximum arm length of 80 m and currently has a single-frequency 10 W Nd:YAG laser [22]. The optical cavity was designed to produce a maximum distortion that is as close as possible to the Advanced LIGO conditions.

To achieve this, we use a Fabry-Perot cavity with a reversed input mirror so that the high reflective coating is on the outside. This allows high power $\sim$1 kW to traverse the substrate. The layout of the experiment is shown in Fig. 2 and the parameters of the cavity are listed in Table I. An intracavity compensation plate (CP) placed within the cavity is conductively heated on its cylindrical surface and is located near the ITM. While the CP in our experiment is directly mounted on a breadboard, in an advanced detector it would be suspended and radiatively heated to avoid noise coupling. The measured cavity lifetime was about 118 ms, giving a finesse of about 1400. The transmitted beam observed with a CCD camera was used to characterize the thermal lens development.

The thermal lensing arises from radial temperature gradients in the test mass due to the Gaussian profile laser beam and radiative heat dissipation through the sides of the mirror. This produces a net radial heat flow. The thermal variation of the material refractive index and the elastic thermal expansion at the mirror surfaces are the two dominant thermal aberrations. Hello and Vinet [13,14] predicted both the steady state and transient temperature distribution throughout a cylindrical mirror for the case where the change in temperature due to absorption of optical power remains small compared to the external ambient temperature. The time evolution of the thermal aberration per unit total absorbed power for a concentric laser beam passing through a cylindrical test mass of radius a and height h, is given by an infinite sum of exponentials as follows:

$$\psi(t, r) = \frac{4\beta a^4}{Kh} \sum_{p,m} \frac{d_m}{\xi_m} [1 - e^{-\alpha_{pm} t}] \left[\frac{1 - \cos(u_p h/a)}{u_p} - \frac{\tau \sin(u_p h/a)}{\xi_m^2 + u_p^2} \right] \frac{J_0(\xi_m r/a)}{c_p u_p}, \quad (1)$$

where $\tau = 4\varepsilon\sigma T_0^3 a/K$. Here ξ_m is mth solution of equation, $xJ_1(x) = \tau J_0(x)$, and u_p is the pth solution of equation, $u = \tau \cot(uh/2a)$. The terms d_m are the coefficients of a Dini series expansion of the azimuthally symmetric incident intensity distribution, while $\alpha_{pm} = \frac{K}{\rho C a^2} \times (\xi_m^2 + u_p^2)$ and $c_p = 1 + \frac{a}{u_p h} \sin(u_p h/a)$ The constants β, K, ε, and ρ are the thermo-optical coefficient, the thermal conductivity, the emissivity, and the density of the test mass material, respectively, and σ is the Stefan-Boltzmann constant. We show below that Eq. (1) can be approximated as a sum of just two exponentials.

To enable modeling of arbitrary geometry we used finite element modeling (FEM) to calculate the time evolution of a thermal lens. Figure 3 compares the time dependent

TABLE I. Parameters of the cavity.

	ITM	ETM	CP
Radius of curvature (m)	$R_1 = \infty$	$R_2 = 720$	Flat
Materials	sapphire	sapphire	fused silica
Diameter (mm)	100	150	160
Thickness (mm)	50	80	17
high-reflection coated transmission (ppm)	1840 ± 100	20	
antireflection coated reflectivity (ppm)	29 ± 20	12 ± 12	<100
Cavity internal power (kW)	1.0		
Cavity length (m)	77		

optical path difference between the beam center and the beam waist position calculated using Eq. (1) and a FEM model. We assumed an absorbed power of 0.5 W, corresponding to a substrate absorption coefficient of 50 ppm/cm and 1 kW circulating power.

The analytical results summed over the first 60 terms (dashed line) and the FEM modeling results (asterisks) show excellent agreement. The radius of curvature due to laser beam heating of the ITM substrate is about 2.5 km, even stronger than that expected (4.9 km) for the Advanced LIGO using fused silica as the test mass material [16]. The solid line shown in Fig. 3 is the sum of two exponentials fitted to the FEM model result, with time constants τ_1 and τ_2. This result is clearly a good approximation to both the analytical and FEM results. We interpret τ_1 as due to the time constant for heating the Gaussian beam profile within the test mass, while τ_2 characterizes the much longer time it takes the test mass to radiate heat through its sides and come into steady state equilibrium with the heated beam volume. For our sapphire ITM, we find that $\tau_1 = 0.76$ s and $\tau_2 = 5.91$ s. It is interesting to note that the value of the time constants τ_1 and τ_2 depend slightly on the mirror geometry and so are only valid for this particular ITM. The thermal lensing of the fused silica CP can be similarly modeled, yielding the much longer time constants of $\tau_1 = 7.40$ s and $\tau_2 = 50.1$ s.

The thermal lensing in the ITM causes the beam size on the end test mass (ETM) to change correspondingly. The radius of the beam (ω) on the ETM can be expressed as the function of the laser beam wavelength, the cavity length (L) and the radii of curvature of the ITM (R_1) and ETM (R_2) [23],

$$\omega = \sqrt{\frac{R_2\lambda}{\pi}}\left(\frac{L}{R_2 - L}\right)^{1/4}\left(1 + \frac{R_2}{R_1}\right)^{-1/4}. \qquad (2)$$

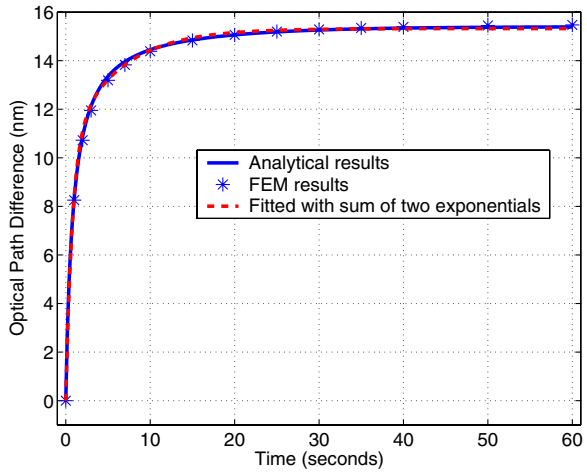

FIG. 3 (color online). Simulation results of ITM thermal lensing time dependence when 0.5 W was absorbed; the dots are simulated results and the solid line is the fitted the curve using the sum of two exponentials with time constants of 0.76 and 5.91 s.

In our case, $R_1 \gg R_2$, and Eq. (2) can be approximated as

$$\omega = \sqrt{\frac{R_2\lambda}{\pi}}\left(\frac{L}{R_2 - L}\right)^{1/4}\left(1 - \frac{R_2}{4R_1}\right). \qquad (3)$$

Equation (3) implies that the beam radius ω reduces linearly with the optical path difference because the latter is directly proportional to $1/R_1$.

Thus we expect the time dependence of ω to follow the sum of exponentials predicted above, with the same time constants. Using the configuration illustrated in Fig. 2, the beam radius at the ETM can be calculated from the measured beam radius on the CCD using Gaussian beam propagation law. The experiment consisted of measuring the beam radius as a function of time since cavity locking. The time dependence of the beam radius at the ETM, and the transmitted power are plotted in Fig. 4. The imaged spots could be accurately described by a fundamental transverse mode Gaussian intensity profile and no obvious asymmetric distortion was observed. The cold-cavity beam radius at the CCD was 1.0 mm, corresponding to the beam radius of 9.3 mm at the ETM. As expected, thermal lensing at the ITM decreases the beam size at the ETM.

Since the time constants for the thermal lensing are known, only 2 free parameters, the powers absorbed by the ITM and CP, are needed to fit the expected time dependence to the measurements. Thus the time evolution of the thermal lens provides a means of measuring the optical absorption of the ITM. The solid line in Fig. 4 shows the fitted time dependence, which yields absorbed powers of 0.51 W and 5.5 mW, respectively. Because the coating absorption is much less than the substrate bulk absorption in the ITM the above absorbed power corresponds to an average bulk absorption of about 51 ppm/cm in the ITM. The power absorbed in the CP is about 5.5 ppm.

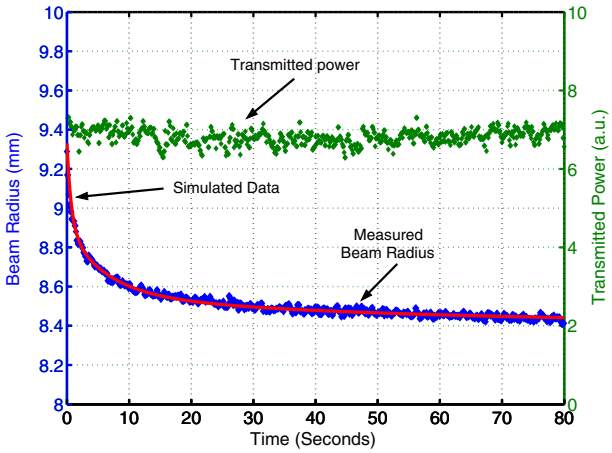

FIG. 4 (color online). A plot of the measured time dependence of the beam radius at the ETM (dots) and the result of a simulation in which only the power absorbed by the ETM and CP were optimized (solid line). The cavity circulating power is shown on the top of the graph.

3

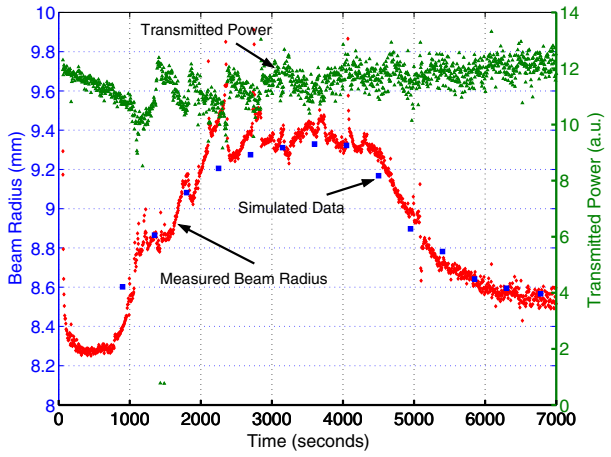

FIG. 5 (color online). Time dependence of the measured (dots) and simulated (squares) ETM beam radius during thermal compensation. Optical power storage commenced at $t = 0$; CP heating power was turned on at 450 s and turned off at time 4026 s. The power transmitted through the ETM, which is proportional to the stored cavity power, is also shown.

Thermal compensation was simulated using a model similar to that used for the simulation of the thermal lensing with the addition of heating from the heating ring. The results, shown as squares in Fig. 5, agree reasonably well with the measurements.

In conclusion, we have observed significant wave front distortion due to optical absorption in the substrate of a mirror, using conditions that are traceable to those expected in the Advanced LIGO. The observed distortion is consistent with that expected from modeling, and could lead to a significant reduction in sensitivity and perhaps instrument failure. The time evolution of thermal lensing shows a double exponential dependence in agreement with the predictions of our finite element model [12] and the analytical model of Vinet and Hello [13]. Measurement of the thermal time constants allow an accurate estimate of the test mass optical absorption. We have also shown that the distortion can be compensated using a conductively heated, fused silica compensation plate. Furthermore, it appears feasible that the compensation could be maintained using a system in which the transmitted beam size is used to define an error signal for feedback control.

An off-axis Hartmann wave front sensor will shortly be installed at the HOPTF, which will allow spatially resolved, sensitive measurements of the wave front distortion in the ITM and CP [24]. An autoalignment system [20] will be implemented to prevent the thermal drift effects observed in Fig. 5.

We would like to thank the International Advisory Committee of the ACIGA/LIGO High Power Test Facility for their encouragement and advice. This research was supported by the Australian Research Council and the Department of Education, Science and Training and by the U.S. National Science Foundation. It is a project of the Australian Consortium for Interferometric Gravitational Astronomy in collaboration with LIGO. We thank especially Barry Barish, Stan Whitcomb, and David Reitze whose support made this project possible.

[1] B. Abbott *et al.* (LIGO Scientific Collaboration), Phys. Rev. Lett. **94**, 181103 (2005).
[2] B. Abbott *et al.* (LIGO Scientific Collaboration), Phys. Rev. Lett. **95**, 221101 (2005).
[3] B. Abbott *et al.* (LIGO Scientific Collaboration), Phys. Rev. D **73**, 062001 (2006).
[4] B. Abbott *et al.* (LIGO Scientific Collaboration), Phys. Rev. D **72**, 122004 (2005).
[5] B. Abbott *et al.* (LIGO Scientific Collaboration), Phys. Rev. D **69**, 082004 (2004).
[6] C. Cutler and K. S. Thorne, *Proceedings of the 16th International Conference on General Relativity Gravity* (2002), p. 72.
[7] P. Fritschel, http://www.ligo.caltech.edu/docs/T/T010075-00.pdf.
[8] C. Zhao, L. Ju, J. Degallaix, S. Gras, and D. Blair, Phys. Rev. Lett. **94**, 121102 (2005).
[9] W. Winkler, K. Danzmann, A. Rüdiger, and R. Schilling, Phys. Rev. A **44**, 7022 (1991).
[10] R. C. Lawrence, http://www.ligo.caltech.edu/docs/P/P030001-00.pdf.
[11] R. Lawrence, M. Zucker, P. Fritschel, P. Marfuta, and D. Shoemaker, Classical Quantum Gravity **19**, 1803 (2002).
[12] J. Degallaix, C. Zhao, L. Ju, and D. Blair, Appl. Phys. B **77**, 409 (2003).
[13] P. Hello and J. Vinet, J. Phys. (France) **51**, 1267 (1990).
[14] P. Hello and J. Vinet, J. Phys. (France) **51**, 2243 (1990).
[15] Ryan Lawrence, David Ottaway, Peter Fritschel, and Mike Zucker, Opt. Lett. **29**, 2635 (2004).
[16] J. Degallaix, Ph.D. thesis, The University of Western Australia, 2006 (to be published).
[17] D. Ottaway, K. Mason, S. Ballmer, M. Smith, P. Willems, C. Vorvick, G. Moreno, and D. Sigg, http://www.ligo.caltech.edu/docs/G/G050095-00/G050095-00.pdf.
[18] D. J. Ottaway, J. Betzwieser, S Ballmer, S. Waldman, and W. Kells, Opt. Lett. **31**, 450 (2006).
[19] H. Luck, A. Freise, S. Gosler, S. Hild, K. Kawabe, and K Danzmann, Classical Quantum Gravity **21**, S985 (2004).
[20] B. J. Slagmolen, M. Barton, C. Mow-Lowry, G. de Vine, D. S. Rabeling, J. H. Chow, A. Romann, C. Zhao, M. B. Gray, and D. E. McClelland, Gen. Relativ. Gravit. **37**, 1601 (2005).
[21] L. Ju *et al.*, Classical Quantum Gravity **21**, S887 (2004).
[22] D. Hosken, D. Mudge, C. Hollitt, K. Takeno, P. Veitch, M. Hamilton, and J. Munch, Prog. Theor. Phys. Suppl. **151**, 216 (2003).
[23] A. E. Siegmann, *Lasers* (University Science Books, Sausalito, California).
[24] A. Brooks, P. Veitch, J. Munch, and T.-L. Kelly, Gen. Relativ. Gravit. **37**, 1575 (2005).

4